JGR Biogeosciences

RESEARCH ARTICLE
10.1029/2026JG009686

Siderophores Reshape Microbial Fe(III) Reduction and Arsenic Release From Iron (Oxyhydr)Oxides

Si Meng Li[1,2], Wei Xiu[1,3], Xi Yang Xu[4], Jin Xing Xie[5], Zhi Xin Fang[1,2], Di Zhang[1,2], Jonathan R. Lloyd[5], Andreas Kappler[4], and Hua Ming Guo[1,2]

[1]State Key Laboratory of Geomicrobiology and Environmental Changes (GMEC), China University of Geosciences (Beijing), Beijing, China, [2]MOE Key Laboratory of Groundwater Circulation and Environment Evolution, School of Water Resources and Environment, China University of Geosciences (Beijing), Beijing, China, [3]Institute of Earth Sciences, China University of Geosciences (Beijing), Beijing, China, [4]Geomicrobiology, Department of Geosciences, University of Tübingen, Tübingen, Germany, [5]Williamson Research Centre for Molecular Environmental Science, School of Earth and Environmental Sciences, The University of Manchester, Manchester, UK

Abstract High-arsenic (As) groundwater is a global environmental concern, with As release largely governed by microbial reductive dissolution of Fe(III) (oxyhydr)oxides. Dissolved organic matter (DOM) rich in Fe-complexing ligands can modify these reactions, yet its influence on Fe(III) (oxyhydr)oxides transformation and associated As mobility remains poorly constrained. Here, we investigated the microbial reduction of As-bearing goethite by *Shewanella oneidensis* MR-1 in the presence of the hydroxamate siderophore desferrioxamine B (DFOB), used as a model strong Fe-complexing organic ligand, Luria–Bertani rather than a compositional analogue of bulk DOM. Results showed that DFOB markedly enhanced microbial Fe(III) reduction, increasing initial reduction rates by up to 70% and total Fe(II) production by 24% relative to MR-1-only controls. This acceleration stemmed from DFOB-facilitated Fe(III) complexation and improved electron-transfer interactions between MR-1 and goethite. Arsenic release occurred in all treatments and was positively correlated with the amount of reacted Fe (dissolved plus reduced Fe), indicating coupled Fe-As redox cycling. Despite stimulating Fe(III) reduction, DFOB did not promote additional As release, with MR-1-DFOB treatments exhibiting As mobilization similar to MR-1-only controls. This constrained As release was likely associated with DFOB-mediated redistribution of biogenic Fe(II) into solid-associated Fe pools and secondary Fe-rich phases, including locally observed nano-magnetite, minor siderite, and possibly poorly crystalline Fe phases, which may have contributed to As retention through adsorption and coprecipitation. These results reveal that DOM rich in Fe-complexing ligands, such as siderophores, can promote the formation of As-sequestering Fe-mineral phases, uncovering an unrecognized control on Fe-As interactions that may shape groundwater As mobilization.

Plain Language Summary Arsenic in groundwater is a major threat to drinking water safety in many parts of the world. It often enters groundwater when microorganisms break down Fe minerals in sediments that naturally hold As. Organic matter in groundwater can affect this process because it can feed microorganisms and bind with iron. In this study, we examined how a strong iron-binding molecule, a hydroxamate siderophore desferrioxamine B (DFOB), changes As release during these reactions. Using laboratory experiments with an As-bearing iron mineral, we found that DFOB helped microorganisms react with the mineral faster and increased Fe transformation. However, it did not cause more As to accumulate in the water. Instead, some of the released Fe appeared to be redistributed into Fe-rich solids, such as locally observed nano-magnetite, minor siderite, and possibly poorly crystalline Fe phases, which may have helped retain part of the As. This shows that organic molecules in groundwater may speed up iron reactions without always increasing As contamination. The final outcome depends not only on how much Fe is broken down but also on whether newly formed Fe minerals form and trap As before it can remain in groundwater.

Key Points:

- DFOB significantly enhanced microbial Fe(III) reduction of As-bearing goethite
- Arsenic release was positively correlated with the amount of reacted Fe
- DFOB induced formation of secondary Fe minerals that retain arsenic

Supporting Information:

Supporting Information may be found in the online version of this article.

Correspondence to:

W. Xiu and H. M. Guo,
xwsuron@cugb.edu.cn;
hmguo@cugb.edu.cn

Citation:

Li, S. M., Xiu, W., Xu, X. Y., Xie, J. X., Fang, Z. X., Zhang, D., et al. (2026). Siderophores reshape microbial Fe(III) reduction and arsenic release from iron (Oxyhydr)oxides. *Journal of Geophysical Research: Biogeosciences*, *131*, e2026JG009686. https://doi.org/10.1029/2026JG009686

Received 8 JAN 2026
Accepted 13 JUL 2026

Author Contributions:

Conceptualization: Si Meng Li, Wei Xiu
Data curation: Si Meng Li, Wei Xiu, Xi Yang Xu, Jin Xing Xie, Zhi Xin Fang
Formal analysis: Si Meng Li, Wei Xiu, Xi Yang Xu, Jin Xing Xie
Funding acquisition: Wei Xiu, Di Zhang, Hua Ming Guo
Investigation: Si Meng Li, Wei Xiu, Zhi Xin Fang
Methodology: Si Meng Li, Wei Xiu, Xi Yang Xu, Jin Xing Xie, Zhi Xin Fang
Supervision: Wei Xiu, Hua Ming Guo
Visualization: Si Meng Li, Wei Xiu, Xi Yang Xu, Jin Xing Xie, Zhi Xin Fang
Writing – original draft: Si Meng Li, Wei Xiu
Writing – review & editing: Si Meng Li, Wei Xiu, Jonathan R. Lloyd, Andreas Kappler, Hua Ming Guo

1. Introduction

High arsenic (As) groundwater, frequently exceeding the World Health Organization guideline of 10 μg L^{-1}, poses a major global health threat (Mukherjee et al., 2024; Podgorski & Berg, 2020). Arsenic mobilization in reducing aquifers is fundamentally driven by the microbial reductive dissolution of As-bearing Fe(III) (oxyhydr)oxide minerals (Cai et al., 2021; Lopez-Adams et al., 2021). Dissolved organic matter (DOM) plays a

critical role in controlling this process through its multifaceted interactions with both microbes and minerals (Glodowska et al., 2020; Mladenov et al., 2015; Wang et al., 2021).

DOM is a key reactive constituent in aquifers that shapes Fe redox cycling through multiple interacting mechanisms. It fuels microbial respiration as an electron donor, mediates electron transfer via redox-active moieties, and forms strong complexes with Fe species (Melton et al., 2014; Qiao et al., 2021). For example, humic substances and aquifer-derived DOM can enhance Fe(III) reduction by serving as both electron donors and shuttles, thereby stimulating the release of As from sediments (Cai et al., 2021; Feng et al., 2025). Beyond these redox functions, the strong complexing capacity of DOM can directly dissolve As-bearing Fe(III) (oxyhydr)oxide minerals, promoting the release of Fe(III)-DOM complexes that are more bioavailable to Fe-reducing microorganisms (Li et al., 2025; X. Liu et al., 2017). DOM can also stabilize biogenic Fe(II) through complexation, preventing its sorption onto minerals and altering mineral transformation pathways (H. L. Dong et al., 2023; Sheng et al., 2024; ThomasArrigo et al., 2018). The overall impact of DOM depends on the balance between Fe(II) and Fe(III) complexation, which governs whether Fe(II) accumulates, precipitates, or drives further reduction reactions (H. L. Dong et al., 2023; Urrutia et al., 1999). However, the synergistic effects of organic ligands and microbial Fe(III) reduction, particularly how ligand-induced dissolution interacts with microbial reductive processes to influence mineral transformation and As mobility, remain poorly understood.

In natural aquifers, organic ligands, including microbially secreted siderophores, intersect with Fe and As cycling through intertwined chemical and biological pathways (Aftabtalab et al., 2022). Siderophores, continuously secreted by bacteria and fungi (Kramer et al., 2020), persist in porewaters and DOM pools at nanomolar to micromolar levels (Tomczyk-Żak et al., 2013), and contribute disproportionately to the Fe-binding and redox capacity of DOM (Boiteau et al., 2016). Far beyond their role in microbial Fe acquisition, siderophores actively mediate Fe speciation and transformation; they chelate Fe(III) from mineral surfaces, enhance electron transfer through complexation, and partially stabilize aqueous Fe(II) (Cheah et al., 2003; Simanova et al., 2010; Wang et al., 2015). These processes reshape mineral dissolution-precipitation equilibria and thereby influence the coupled mobilization of Fe and As. Yet, despite their ubiquity and thermodynamic strength, the synergistic coupling between siderophore-driven complexation and microbial Fe(III) reduction remains unexplored in the context of As-bearing minerals. Understanding this interplay is critical for predicting whether organic ligands accelerate As release through Fe solubilization or promote its sequestration within newly formed Fe(II) minerals.

During microbial Fe(III) reduction, biogenic Fe(II) accumulates in solution and at mineral surfaces, where it drives secondary mineral formation through several coupled pathways, including precipitation with dissolved anions, adsorption-induced interfacial electron transfer, and subsequent dissolution-reprecipitation or recrystallization of the parent Fe(III) (oxyhydr)oxides. At ambient temperatures, Fe(II)-bearing phases such as magnetite and green rust commonly form through dissolution–reprecipitation processes, whereas carbonate- or phosphate-bearing phases such as siderite and vivianite can form through precipitation with dissolved anions (Y. R. Dong et al., 2020; Han et al., 2018; O'Loughlin et al., 2013; Usman et al., 2018). These secondary Fe(II) minerals sequester As either through surface adsorption or by incorporation into their crystal structures, thereby influencing its long-term mobility in groundwater (Jiang et al., 2013; Tufano & Fendorf, 2008). The rate of Fe(III) reduction controls the crystallinity and stability of secondary Fe(II) minerals: rapid reduction produces metastable phases such as green rust that transiently retain As, whereas slower reduction forms crystalline magnetite and siderite that stably sequester As (Amstaetter et al., 2010, 2012; Piepenbrock et al., 2011; Zachara et al., 1998). In addition, mineralogical factors such as crystal facet reactivity influence these processes (Barrón & Torrent, 1996; Hua et al., 2022; Klyukin et al., 2018; Livi et al., 2023; Rubasinghege et al., 2010). Facets enriched in singly coordinated Fe sites, such as the (021) plane of goethite (Klyukin et al., 2018; Zhang et al., 2021), are highly reactive interfacial sites and serve as hotspots for Fe(II) adsorption and nucleation. The adsorbed Fe(II) catalyzes lattice reconstruction and magnetite formation (Usman et al., 2013), but this process can be inhibited by organic ligands that strongly complex Fe(II), suppressing secondary mineral crystallization (ThomasArrigo et al., 2018). Consequently, the competition between Fe(II)-ligand complexation and Fe(II)-induced mineral transformation dictates whether Fe(III) reduction leads to As release or retention. However, it remains unclear whether a strong Fe-binding siderophore can enhance microbial Fe(III) reduction while limiting net dissolved As accumulation by redirecting biogenic Fe(II) into As-retentive secondary Fe phases.

This study investigates how ligand complexation modulates microbial Fe(III) reduction kinetics and As mobilization during the interaction between the Fe-reducing bacterium *Shewanella oneidensis* MR-1 and As-bearing

Table 1
Experimental Series and Corresponding Abbreviations Used in This Study

Experimental condition	Goethite (Gt) series	As(V)-Gt series	As(III)-Gt series
Control (no *Shewanella oneidensis* MR-1 or DFOB)	Gt	As(V)-Gt	As(III)-Gt
DFOB-only	Gt-DFOB	As(V)-Gt-DFOB	As(III)-Gt-DFOB
Shewanella oneidensis MR-1-only (MR-1)	Gt-MR-1	As(V)-Gt-MR-1	As(III)-Gt-MR-1
Shewanella oneidensis MR-1 + DFOB (MR-1-DFOB)	Gt-MR-1-DFOB	As(V)-Gt-MR-1-DFOB	As(III)-Gt-MR-1-DFOB

goethite. We used the hydroxamate siderophore desferrioxamine B (DFOB) as a model organic ligand representative of the Fe-complexing fraction of DOM. Batch incubation experiments were conducted under anoxic conditions to quantify microbial Fe(III) reduction, As release, and secondary mineral formation in the presence and absence of DFOB. High-resolution Transmission electron microscopy (TEM) and Mössbauer spectroscopy were applied to characterize the nanoscale mineral transformations and Fe(II) speciation. The combined biotic and ligand-controlled systems provide new insights into how organic complexation regulates Fe redox cycling, secondary mineral formation, and As redistribution. These findings advance the mechanistic understanding of how Fe-complexing DOM modulates the coupled microbial and geochemical processes that control As mobility in groundwater.

2. Materials and Methods

2.1. Goethite Synthesis and Characterization

Goethite was synthesized according to the method of Schwertmann and Cornell (2000). Arsenic-bearing goethite was prepared by equilibrating freshly synthesized goethite with As(V) or As(III) solutions, resulting in final As loadings of 9.3 mg g^{-1} (As(V)-Gt) and 10.9 mg g^{-1} (As(III)-Gt), respectively. Detailed synthesis and adsorption procedures are provided in the Supporting Information. X-ray diffraction confirmed the formation of well-crystallized goethite with no detectable secondary phases (Figure S1 in Supporting Information S1), while specific surface area (41.0 ± 0.6 m^2 g^{-1}) and particle morphology were characterized by BET and scanning electron microscopy (SEM) (Figure S2 in Supporting Information S1), respectively.

2.2. Microbial Fe(III) Reduction Experiments

Shewanella oneidensis MR-1, a model Fe(III)-reducing bacterium incapable of reducing As(V), was used in microbial Fe(III) reduction experiments (Muehe et al., 2013). The strain was grown to late-log phase in Luria–Bertani broth at 30°C. The cells were harvested by centrifugation at 6,000 g for 10 min, washed 3 times with piperazine-N,N'-bis(2-ethanesulfonic acid) (PIPES) buffer (10 mM, pH 7), and resuspended in PIPES buffer before inoculation.

Batch Fe(III) bioreduction experiments were performed anaerobically at 25°C in triplicate under four conditions: (a) abiotic control (no *Shewanella oneidensis* MR-1 (MR-1) or desferrioxamine B (DFOB); Gt-only), (b) DFOB-only (Gt-DFOB), (c) *Shewanella oneidensis* MR-1-only (Gt-MR-1), and (d) combined *Shewanella oneidensis* MR-1 with DFOB (Gt-MR-1-DFOB). The abbreviations used to represent different experimental series in the text are summarized in Table 1. Each 100 mL serum bottle contained 1 g L^{-1} mineral, 10 mM PIPES buffer (pH 7.0, autoclaved), 10 mM sodium lactate (electron donor, filter-sterilized), and, when applicable, 0.5 mM DFOB (filter-sterilized) and *Shewanella oneidensis* MR-1 cells (2×10^8 cells mL^{-1}). The final suspension volume was 50 mL. All preparations were conducted in an anoxic glovebox (N_2/H_2, 97.5/2.5 v/v; Coy Laboratory Products, Grass Lake, MI, USA). Solutions were prepared with deoxygenated Milli-Q water (18.2 MΩ cm^{-1}) and purged with N_2 prior to use. Serum bottles were wrapped in aluminum foil to prevent photoreduction. At designated time points (0, 3, 6, 9, 24, 48, 96, 144, and 216 hr), 100 µL of suspension was withdrawn anoxically and added to 0.9 mL of deoxygenated 2 M HCl for total Fe(II) determination. 2 mL of suspension was withdrawn anoxically, filtered through 0.22 µm polyethersulfone (PES) syringe filters, and acidified with HCl for analysis of dissolved Fe(II), total dissolved Fe and dissolved As.

2.3. Aqueous Chemical Analyses

The total dissolved Fe(II) concentration was measured using the spectrophotometric Ferrozine assay (Stookey, 1970). Accurate quantification of total Fe(II) (including aqueous Fe(II) and structural Fe(II)) using the 1,10-phenanthroline method in H_2SO_4-HF digestates was not feasible in the presence of DFOB (Amonette & Templeton, 1998), as the DFOB produces strongly reducing hydroxylamine species under acidic and boiled conditions, leading to substantial overestimation of Fe(II) concentrations (Simanova et al., 2010). Therefore, the total Fe(II) concentration (including aqueous Fe(II) and structural Fe(II)) was extracted in 2 M HCl and measured with the Ferrozine assay (J. Liu et al., 2022). However, the HCl extraction did not fully recover all solid-phase Fe(II), particularly from more crystalline phases, with an estimated extraction efficiency of approximately 76.5 ± 2.50% (Figure S3 in Supporting Information S1). Total dissolved Fe and As were analyzed with inductively coupled plasma-optical emission spectrometry (ICP-OES, Thermo, USA). High-performance liquid chromatography-atomic fluorescence spectrometry (HPLC-AFS, Jitian Corp., Beijing) was used to determine As speciation. Dissolved DFOB concentration was measured using the $FeCl_3$ method (Cheah et al., 2003).

2.4. Mineralogical Characterization

XRD was used to determine the mineralogical phase transformations of goethite before and after the microbial reduction. Scanning electron microscopy and TEM were employed to observe mineralogical changes in mineral structures and potential associations of As with goethite. TEM and scanning transmission electron microscopy (STEM) analyses were conducted using a probe corrected Thermo Fisher Titan G2 80–200 to investigate the morphology and structural features of the bioreduced mineral products. The STEM was equipped with an Energy Dispersive X-ray Spectroscopy (EDS) detector (0.7 steradian solid angle) and a high-angle annular dark field (HAADF) detector. Imaging was carried out at an accelerating voltage of 200 kV, with a STEM convergence angle of 21 mrad, and HAADF signals were collected using an inner collection angle of 55 mrad. Elemental distributions of Fe, As, O, and C were analyzed through EDS elemental mapping in STEM mode. Fast Fourier transform patterns generated from the HRTEM images were used to determine the d-spacing. For sample preparation, the solid samples were suspended with absolute ethyl alcohol and sonicated for 5 min and subsequently pipetted onto 200 mesh copper grids coated with an amorphous carbon film. Mössbauer Spectroscopy was used to further characterize Fe mineral phases and to distinguish among different types of secondary Fe minerals. For Mössbauer measurements, dried solid powders were prepared in an anoxic glovebox and loaded into Plexiglas holders with area of 1 cm^2, forming a thin disc. Spectra were collected at both 140 and 77 K using a constant acceleration drive system (WissEL) in transmission mode with a ^{57}Co/Rh source. The X-ray photoelectron spectroscopy (XPS) was used to explore the chemical composition and valent state of Fe and As before and after reduction.

2.5. Statistical Analysis

The initial fast microbial Fe(III) reduction rate was calculated based on the first 48 hr according to previous studies (Muehe et al., 2013; Zhang et al., 2022). Two-way ANOVA was used to assess the statistical significance of differences among treatments, with $p < 0.05$ considered significant.

3. Results and Discussion

3.1. DFOB-Enhanced Microbial Reduction and Dissolution of As-Bearing Goethite by *Shewanella oneidensis* MR-1

The influence of the siderophore desferrioxamine B (DFOB) on the kinetics of microbial Fe(III) reduction was examined using goethite and As-bearing goethite under biotic and abiotic conditions. In the absence of *Shewanella oneidensis* MR-1, no detectable Fe(II) accumulation occurred in controls with or without DFOB, confirming that abiotic reductive dissolution of goethite or As-bearing goethite by DFOB was negligible, which was consistent with previous studies (Reichard et al., 2007; Wang et al., 2015). In contrast, inoculation with *Shewanella oneidensis* MR-1 led to clear Fe(II) accumulation (Figures 1a–1c), indicating active microbial Fe(III) reduction. The kinetics of microbial Fe(III) reduction followed a biphasic pattern, with a rapid initial phase during the first 48 hr followed by a slower stage over the next 168 hr (Figures 1a–1c), consistent with previous reports of declining Fe(III) (oxyhydr)oxide reducibility over time (Fritzsche et al., 2021; Xu et al., 2025).

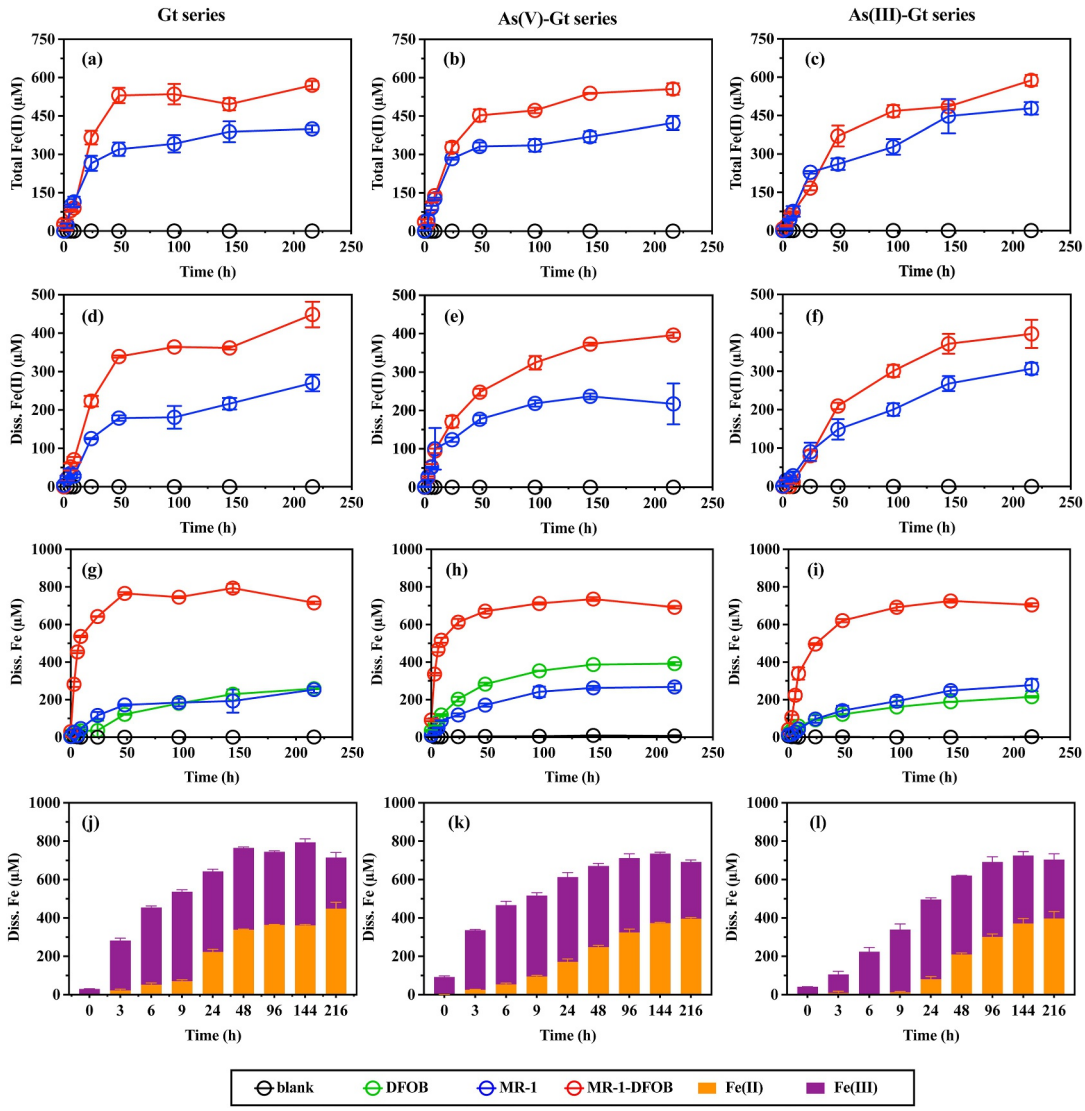

Figure 1. Time course of total Fe(II), total dissolved Fe(II), total dissolved Fe, and dissolved Fe species during microbial reduction of (a, d, g, and j) Gt, (b, e, h, and k) As(V)-Gt, and (c, f, i, and l) As(III)-Gt by *Shewanella oneidensis* MR-1 in the presence or absence of 500 μM DFOB.

The presence of DFOB markedly enhanced both the rate and extent of microbial Fe(III) reduction (Figures S4 and S6 in Supporting Information S1). In the goethite series, the initial reduction rate increased from 6.68 ± 0.32 μmol h^{-1} g^{-1} in Gt-MR-1 to 11.04 ± 0.36 μmol h^{-1} g^{-1} in Gt-MR-1-DFOB (two-way ANOVA, $p < 0.0001$), while cumulative Fe(II) production after 216 hr rose from 399.46 ± 8.20 to 570.13 ± 9.49 μM ($p < 0.0001$) (Table S1 in Supporting Information S1). This enhancement reflects the formation of dissolved Fe (III)-DFOB complexes that increase Fe(III) bioavailability for microbial reduction (Kuhn et al., 2014). Moreover, Fe(III) release during the first 24 hr was higher in Gt-MR-1-DFOB than in the abiotic Gt-DFOB control (Figure 1j), indicating a catalytic role of biogenic Fe(II) in ligand-promoted dissolution. It was reported that micromolar Fe(II), whether biogenic or abiogenic, could act as a redox-active catalyst by transferring electrons to surface Fe(III), accelerating the release of Fe(III)-ligand complexes by 10 ∼ 40 fold (Biswakarma et al., 2019, 2020, 2021; Carrasco et al., 2007). The observed acceleration therefore results from a synergistic interplay between Fe(III)-DFOB complexation and Fe(II)-mediated redox cycling, where DFOB facilitates interfacial Fe(II)-Fe(III) electron transfer and sustains Fe(III) bioavailability. Because all experiments were conducted at circumneutral pH, partial protonation of hydroxamate groups in Fe(III)-DFOB complexes is expected, which increases their reduction potential and makes them more susceptible to microbial electron transfer than solid

Fe(III) (Kim et al., 2010). Collectively, these results show that DFOB enhances microbial Fe(III) reduction by simultaneously increasing Fe(III) solubility and accelerating interfacial redox cycling.

Arsenic speciation exerted distinct effects on microbial Fe(III) reduction by *Shewanella oneidensis* MR-1. The oxidation state of As remained unchanged in both As(V)-Gt and As(III)-Gt after microbial reduction. In As(V)-Gt series, the initial reduction rate (6.91 ± 0.19 μmol h^{-1} g^{-1}) and total Fe(II) production (423.74 ± 16.07 μM) were comparable to those in the As-free goethite series ($p > 0.05$) (Figures S5, S7 and Table S1 in Supporting Information S1), indicating that As(V) adsorption exerted negligible influence on microbial Fe(III) reduction. This contrasts with ferrihydrite systems, where As(V) adsorption can inhibit reduction by forming inner-sphere surface complexes (L. J. Ding et al., 2022; Majzlan, 2011; Wu et al., 2018). In contrast to As(V), the presence of As(III) lowered the initial reduction rate but enhanced the overall extent of microbial Fe(III) reduction (Figures S5 and S7 in Supporting Information S1). In the As(III)-Gt series, the initial reduction rate for As(III)-Gt-MR-1 decreased to 5.43 ± 0.27 μmol h^{-1} g^{-1}, significantly lower than that of Gt-MR-1 (6.68 ± 0.32 μmol h^{-1} g^{-1}; $p = 0.038$) (Table S1 in Supporting Information S1), whereas the cumulative Fe(II) yield increased from 399.46 ± 8.20 μM in Gt-MR-1 to 478.61 ± 14.25 μM in As(III)-Gt-MR-1 ($p = 0.001$), indicating a slower yet more extensive reduction process. The contrasting behavior of As(III) arises from its combined physiological and geochemical effects. As(III) toxicity suppresses microbial respiration (Shen et al., 2013; Wang et al., 2016), leading to a slower initial Fe(III) reduction rate. However, the greater extent of reduction likely reflects differences in Fe(II) partitioning, although total Fe(II) production was similar between As(V) and As(III). The greater Fe(III) reduction extent in the As(III)-Gt-MR-1 treatment may be related to differences in Fe(II) partitioning and surface passivation. The higher dissolved Fe(II) fraction in As(III)-Gt-MR-1 than that in As(V)-Gt-MR-1 (64.10 ± 0.09% vs. 51.99 ± 9.56%) suggests that less biogenic Fe(II) was retained in solid-associated Fe(II) pools (Figures 1e and 1f). This may have reduced passivating Fe(II)-bearing coatings and helped preserve access to reactive Fe(III) sites (Jaisi et al., 2007; Roden & Urrutia, 2002; Urrutia et al., 1999), although direct mineralogical evidence remains limited. Together, these results show that As(III) slows microbial kinetics through toxicity but ultimately enhances reduction extent by preserving Fe(III) accessibility.

When DFOB and As coexisted, the overall extent of Fe(III) reduction remained similar to the DFOB-only treatments, with total Fe(II) reaching 555.92 ± 13.06 μM for As(V)-Gt-MR-1-DFOB ($p > 0.05$) and 587.62 ± 12.31 μM for As(III)-Gt-MR-1-DFOB ($p > 0.05$) (Figure S5 in Supporting Information S1). However, both As species slowed the reduction kinetics: the initial rate decreased from 11.04 ± 0.36 μmol h^{-1} g^{-1} in Gt-MR-1-DFOB to 9.44 ± 0.29 μmol h^{-1} g^{-1} in As(V)-Gt-MR-1-DFOB ($p = 0.01$) and to 7.72 ± 0.49 μmol h^{-1} g^{-1} in As(III)-Gt-MR-1-DFOB ($p < 0.0001$) (Figure S3 in Supporting Information S1). The slight rate decrease in the As(V)-Gt system likely reflects a combination of surface-site competition and ligand-mediated Fe(III) redistribution. Adsorbed As(V) may compete with DFOB for reactive goethite surface sites and transiently affect surface accessibility. However, our previous experiments showed that Fe dissolution in the As(V)-Gt-DFOB system exceeded that in the Gt-DFOB system (Li et al., 2025), indicating that As(V) did not overall inhibit DFOB-promoted goethite dissolution. Thus, the slower reduction kinetics in the As(V)-Gt-MR-1-DFOB system are unlikely to result solely from a physical barrier effect. Instead, As(V)-associated Fe(III) may need to be redistributed to DFOB-accessible forms before microbial utilization, which could transiently delay reduction kinetics while maintaining overall Fe(III) bioavailability. In contrast, As(III) primarily inhibits reduction through physiological toxicity, disrupting electron transfer rather than Fe(III) speciation (Shen et al., 2013; Wang et al., 2016). Despite these kinetic effects, similar total Fe(II) yields across treatments indicate that DFOB effectively buffers Fe(III) availability, sustaining extensive microbial reduction even in As-bearing systems. These results reveal that ligand exchange and microbial toxicity jointly regulate Fe(III) bioavailability and reduction dynamics, underscoring the role of siderophore-mediated complexation in buffering Fe-As interactions in natural environments.

In our experiments, the solution pH was maintained at 7.0 using PIPES buffer, and no appreciable pH change was observed during microbial reduction. Within the pH range of 2–7, DFOB and Fe(III)-DFOB complexes are predominantly present as positively charged H_4DFOB^+ and $FeHDFOB^+$ species, respectively (Bellotti & Remelli, 2021; Wang et al., 2015). Proton-promoted dissolution of goethite occurs under acidic conditions.

3.2. Arsenic Release During Microbial Fe(III) Reduction

Following the observed Fe(III) reduction dynamics, As release from As-bearing goethite was tracked under abiotic and biotic conditions, with and without DFOB, to determine how microbial reduction and siderophore-

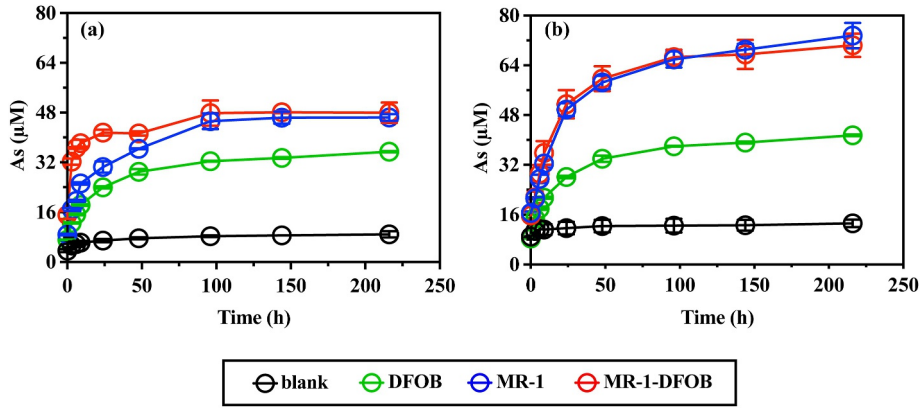

Figure 2. Arsenic release during microbial reduction of (a) As(V)-Gt and (b) As(III)-Gt series by *Shewanella oneidensis* MR-1 in the presence or absence of 500 μM DFOB.

promoted dissolution affect As mobilization. In the abiotic series without DFOB, a rapid initial release of As was observed (Figure 2), with dissolved As concentrations increasing to 8.88 ± 0.75 μM for As(V)-Gt and 13.23 ± 0.87 μM for As(III)-Gt within 48 hr and remaining nearly constant thereafter (Table S2 in Supporting Information S1). This release is attributed to the desorption of surface-bound As into the background electrolyte, consistent with previous reports (Guo et al., 2015; O'Reilly et al., 2001). In contrast, the addition of DFOB markedly enhanced As release, increasing total dissolved As by 3.7 fold for As(V)-Gt and 2.9 fold for As(III)-Gt relative to the DFOB-free controls. This enhancement reflects ligand-promoted dissolution of goethite, in which Fe(III)-DFOB complexation accelerates the detachment of Fe-As surface linkages and facilitates As mobilization, consistent with our previous findings (Li et al., 2025).

In all biotic series, As release was observed as a consequence of reductive dissolution of As(V)-Gt and As(III)-Gt (Figure 2), since *Shewanella oneidensis* MR-1 is not able to use As(V) as a terminal electron acceptor (Jiang et al., 2009, 2013), exhibiting a biphasic pattern with rapid mobilization during the first 48 hr followed by a slower phase. In the As(V)-Gt series, DFOB accelerated the initial rate of As release from 0.76 ± 0.01 μmol h^{-1} g^{-1} for As(V)-Gt-MR-1 to 0.86 ± 0.01 μmol h^{-1} g^{-1} for As(V)-Gt-MR-1-DFOB ($p = 0.049$) (Table S2 in Supporting Information S1), indicating that DFOB facilitated the early dissolution of surface-bound As(V) through enhanced Fe(III) reduction. However, DFOB did not affect the overall extent of As(V) release because the final dissolved As(V) concentrations were comparable to 46.43 ± 0.60 μM for As(V)-Gt-MR-1 and 47.95 ± 1.90 μM for As(V)-Gt-MR-1-DFOB (Figure 2a and Table S2 in Supporting Information S1). In the As(III)-Gt series, DFOB had limited influences on either the rate or extent of As(III) release, with initial As(III) release rate of 1.22 ± 0.03 μmol h^{-1} g^{-1} and 1.24 ± 0.05 μmol h^{-1} g^{-1}, and final As(III) concentrations of 70.43 ± 2.15 μM and 73.56 ± 2.35 μM for As(III)-Gt-MR-1 and As(III)-Gt-MR-1-DFOB (Figure 2b and Table S2 in Supporting Information S1), respectively. Notably, As(III)-Gt-MR-1-DFOB series exhibited both a higher release rate and a greater final dissolved concentration than As(V)-Gt-MR-1-DFOB series. This contrast reflects the weaker binding affinity and greater lability of As(III) relative to As(V) on goethite surfaces. Previous studies confirmed that As(III) exhibits weaker adsorption affinity but a larger capacity compared with that of As(V) (Dixit & Hering, 2003; Huang et al., 2024; Kanematsu et al., 2013). Overall, both MR-1-mediated reduction and DFOB-induced dissolution individually enhanced As mobilization from As-bearing goethite. However, although DFOB promoted microbial Fe(III) reduction in As(V)-Gt-MR-1-DFOB and As(III)-Gt-MR-1-DFOB series relative to their respective MR-1-only series, this enhancement in Fe(III) reduction was not accompanied by a corresponding increase in As release.

To assess how ligand-promoted dissolution and microbial reduction influenced As release, we compared the slopes of the relationships between total dissolved As and reacted Fe (dissolved plus reduced Fe) across treatments. For As(V)-Gt series, the slopes were 0.068 (DFOB-only), 0.087 (MR-1-only), and 0.037 (MR-1-DFOB). For As(III)-Gt series, the slopes were 0.15 (DFOB-only), 0.12 (MR-1-only), and 0.067 (MR-1-DFOB). In both As (V)-Gt and As(III)-Gt series, the MR-1-DFOB series exhibited substantially lower slopes, indicating lower As mobilization per unit of reacted Fe relative to DFOB-only or MR-1-only treatments (Figure 3). To further assess

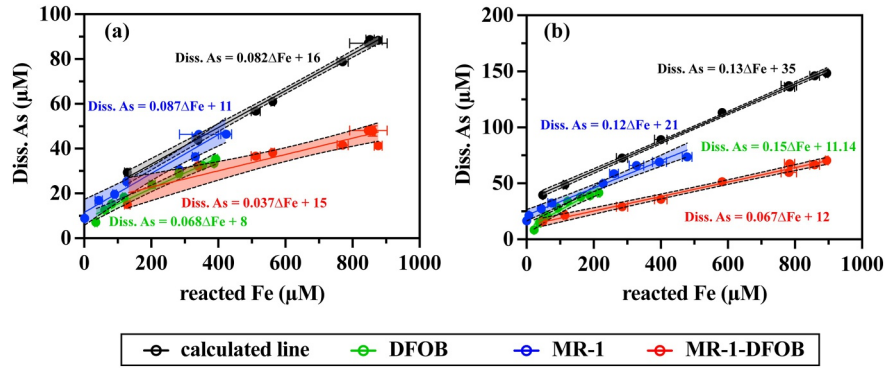

Figure 3. The relationships between As release and reacted Fe in (a) As(V)-Gt and (b) As(III)-Gt series by *Shewanella oneidensis* MR-1 in the presence or absence of 500 μM DFOB. Reacted Fe was defined as total dissolved Fe(III) in the DFOB-only series, total Fe(II) in MR-1-only series, and the sum of total Fe(II) and dissolved Fe(III) in MR-1-DFOB series. The black calculated lines represent the predicted As release in the MR-1-DFOB series under the simplified assumption that ligand-promoted dissolution and microbial reduction contributed independently and additively to As release. These lines were obtained by substituting the experimentally measured total Fe(II) and dissolved Fe(III) concentrations from the MR-1-DFOB series into the regression equations derived from the single-process (DFOB-only and MR-1-only) series.

this discrepancy, the dissolved As concentrations expected for the MR-1-DFOB series were estimated using a simplified additive model derived from the corresponding MR-1-only and DFOB-only treatments. Although microbial Fe(III) reduction and DFOB-promoted dissolution were inherently coupled, their individual contributions could not be quantified separately in the combined series. Under this assumption, the predicted As release (Figure 3, black line) greatly exceeded the observed values in both series. For As(V)-Gt-MR-1-DFOB, 852 μM reacted Fe corresponded to a predicted approximately 89 μM As(V), whereas only 48 μM was measured. For As(III)-Gt-MR-1-DFOB, the predicted about 148 μM As(III) exceeded the measured 70 μM by more than twofold. These differences indicate that approximately 40–80 μM As remained associated with the solid phase, likely sequestered by newly formed Fe(II)-bearing secondary minerals. This interpretation is consistent with previous studies showing that As released during microbial Fe(III) reduction can be partly retained by secondary Fe(II)-bearing minerals, particularly magnetite, through adsorption or structural incorporation (Tufano & Fendorf, 2008; Wu et al., 2018). However, our results further show that even when DFOB enhanced both Fe(III) reduction and Fe dissolution, dissolved As did not increase proportionally, suggesting that DFOB may regulate the redistribution of biogenic Fe(II) into secondary mineral phases and thereby influence As partitioning under coupled ligand-microbe conditions. Overall, the results demonstrate that As mobility cannot be inferred solely from the extent of Fe(III) reduction or ligand-promoted mineral dissolution. Under coupled ligand-microbe conditions, secondary mineral formation exerts strong control over As partitioning, preventing additional As release despite enhanced Fe(III) reduction.

3.3. Secondary Fe Minerals Formed During Microbial Fe(III) Reduction

To elucidate the mineralogical pathways governing Fe and As redistribution, the morphology and composition of residual minerals in biotic treatments with and without DFOB were characterized. High-resolution TEM (HRTEM) analyses were conducted to examine the morphological changes in goethite following microbial reduction. The images revealed that dissolution and reprecipitation were spatially heterogeneous and strongly facet-dependent. Pristine goethite consisted of well-defined rod-shaped crystals (approximately 56 nm wide) with lattice spacings of 0.26 nm for the (021) facet and 0.43 nm for the (110) facet. After microbial reduction, the (021) tips became distinctly roughened, consistent with preferential dissolution along these reactive facets enriched in singly coordinated Fe sites (Figure S9 in Supporting Information S1) (Klyukin et al., 2018; Livi et al., 2017). It has been revealed that microbial reductive dissolution was facet preferential (Hua et al., 2022). Localized dissolution generated Fe(II)-enriched microdomains that served as nucleation centers for secondary mineral formation.

To investigate the type of secondary Fe(II) minerals generated during microbial reduction, high-resolution TEM analyses and Mössbauer spectra were performed. Spherical nanoparticles (5–20 nm) were observed on goethite tips based on SEM and TEM images (Figures 4a and 4b). FFT patterns derived from representative HRTEM

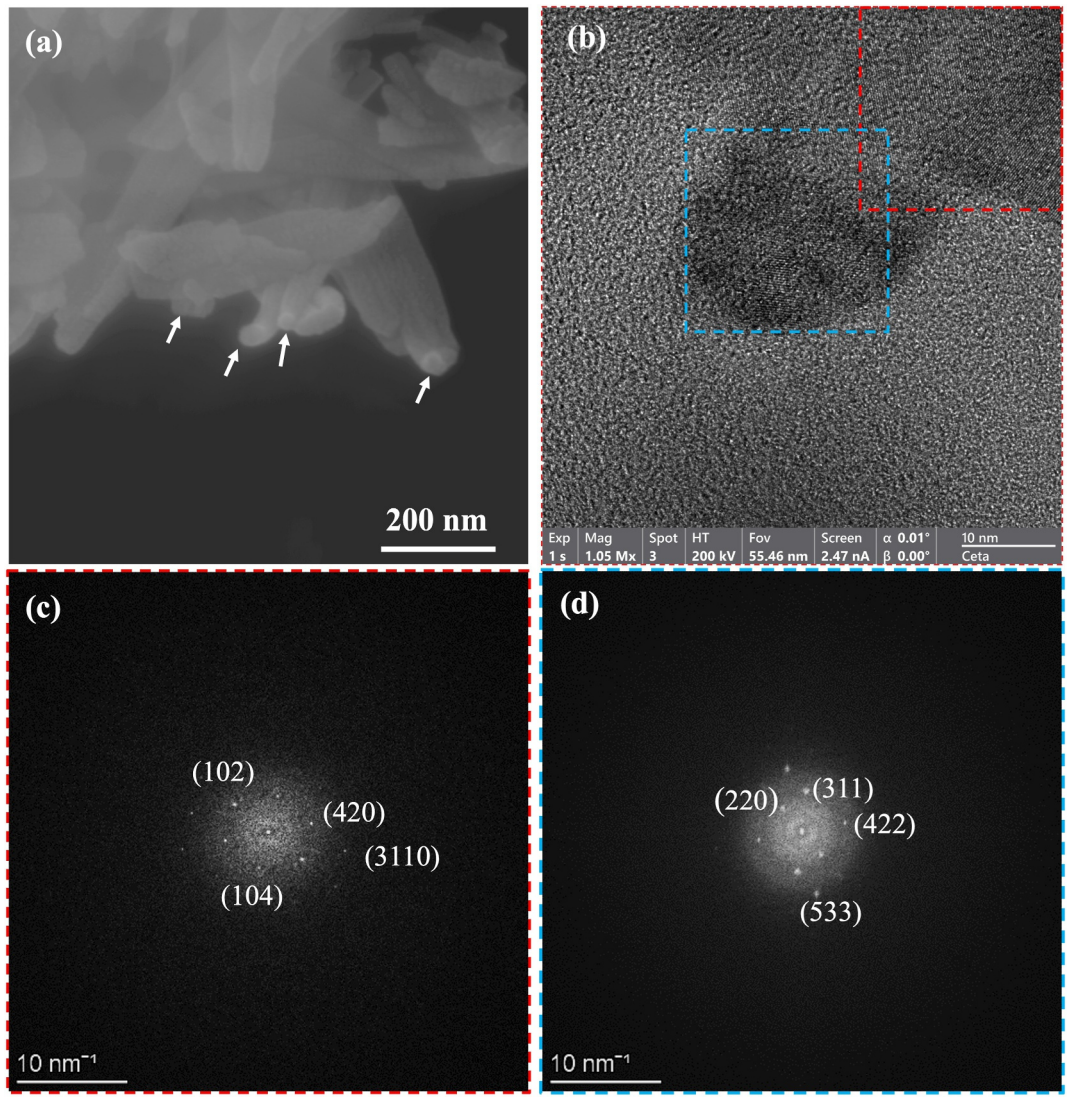

Figure 4. Scanning electron microscopy (SEM) and HRTEM characterization of secondary nanoparticles formed in the As (V)-Gt-MR-1-DFOB series. (a) SEM image showing nanoscale particles associated with the tips and edges of goethite crystals, indicated by white arrows. (b) HRTEM image of a representative nanoparticle-bearing region. (c), (d) Fast Fourier transform patterns derived from the selected regions marked by the red and blue dashed boxes in (b), respectively. The indexed diffraction features in (d) are consistent with magnetite-like secondary nanoparticles. Scale bars: 100 nm in (a) and 10 nm in (b).

images showed reflections of (220), (311), (422), (533), and (442), confirming the presence of magnetite, particularly in the As(V)-Gt-MR-1-DFOB series (Figures 4c and 4d, Table S3 in Supporting Information S1). Magnetite was preferentially observed at the roughened tips of goethite, particularly in regions associated with the reactive (021) facets, indicating that these sites were important for secondary mineral formation (Fredrickson et al., 1998; Lovley, 1991). This spatial association is consistent with Fe(II)-driven interfacial transformation during microbial reduction. In addition, magnetite formation may also have involved dissolution-reprecipitation processes mediated by cell-derived organics, including extracellular polymeric substances, which can influence Fe(II) complexation, labile Fe(III) generation, and the nucleation of secondary Fe minerals (Perez-Gonzalez et al., 2010; Sheng et al., 2024). Chelation of Fe(II) by DFOB inhibited crystal coalescence, stabilizing magnetite at the nanoscale. Complexation of Fe species by DOM is known to modulate Fe(II)-catalyzed transformations by binding labile Fe(III) intermediates and altering olation-oxolation pathways (Y. F. Ding et al., 2024; Sheng et al., 2020). The formation of Fe(II)-DFOB complexes likely retarded Fe(II)-driven recrystallization, delaying bulk precipitation and maintaining small reactive nanoparticles. The resulting nano-magnetite possessed high

surface reactivity and As affinity, with reported sorption capacities of 5.96–16.1 mg g^{-1} for As(V) (Gimenez et al., 2007; C. H. Liu et al., 2015; Yean et al., 2005), and 16.7–29.2 mg g^{-1} for As(III) (Tables S5 and S6 in Supporting Information S1) (Dixit & Hering, 2003; Gimenez et al., 2007; C. H. Liu et al., 2015; Yean et al., 2005), contributing to As retention despite enhanced Fe(III) dissolution induced by DFOB. However, given its low abundance, nano-magnetite is not interpreted here as the sole sink for retained As, but rather as one component of the newly formed Fe(II)-bearing secondary phases that contributed to As sequestration in MR-1-DFOB series.

Mössbauer spectra collected at 140 and 77 K suggested the presence of an additional Fe(II)-bearing component in the DFOB-amended treatments, which was fitted as siderite (Figure 5). In MR-1-only series, spectra were dominated by goethite sextets (CS = 0.46–0.48 mm s^{-1}, $\varepsilon = -0.13$ to -0.11 mm s^{-1}, H = 48.2–49.7 T) (Murad & Cashion, 2004). In contrast, the MR-1-DFOB series displayed two goethite sextets along with an additional doublet assigned to siderite. The goethite sextets in the MR-1-DFOB series exhibited broader parameter ranges (CS = 0.42–0.54 mm s^{-1}, $\varepsilon = -0.21$ to -0.09 mm s^{-1}, H = 46.5–49.7 T), indicating structural modification through Fe(II) incorporation, consistent with previous reports of increased ε in Fe(II)-reacted goethite (Latta et al., 2012). The stability constants of Fe(III)-DFOB and Fe(II)-DFOB were 10^{32} and $10^{10.3}$, respectively (Boukhalfa & Crumbliss, 2002; Cheah et al., 2003; Spasojević et al., 1999). In the MR-1-DFOB series, DFOB preferentially complexed dissolved Fe(III), leaving a substantial portion of microbially produced Fe(II) uncomplexed. This unbound Fe(II) readily precipitated as a siderite, facilitated by microbial lactate metabolism (Pinchuk et al., 2011). The siderite doublet accounted for only 1.2%–1.5% of the total spectral area, which is consistent with the low amount of solid-phase Fe(II) in our study. Siderite possesses high surface reactivity and strong affinity for As through both adsorption and coprecipitation, with reported capacities of 8.4–10.7 mg g^{-1} for As(V) (Guo, Ren, et al., 2013; Yu et al., 2022, 2023), and 5.34–10.2 mg g^{-1} for As(III) (Guo et al., 2011, Guo, Ren, et al., 2013; Yu et al., 2024) (Tables S5 and S6 in Supporting Information S1).

The contrasting detectability of magnetite and siderite across techniques reflects their differing abundance, crystallinity, and formation pathways during microbial reduction. Magnetite was identified primarily from HRTEM observations of nanoscale particles associated with goethite tips, whereas a distinct magnetite component was not resolved in the Mössbauer fits. This suggests that magnetite was present at low abundance or in a nanoscale heterogeneous form below the quantitative resolution of bulk Mössbauer fitting in these samples (Kuzmann et al., 2003). Previous studies have shown that magnetite can serve as a precursor to siderite formation during microbial Fe reduction (H. L. Dong et al., 2000; Han et al., 2024). Mössbauer spectroscopy clearly detected siderite, but it was not readily resolved in TEM images, most likely due to its low abundance and poor crystallinity. Siderite formed as fine, dispersed precipitates in carbonate-enriched microenvironments, whereas magnetite nucleated directly on goethite surfaces, producing well-crystallized nanoparticles readily captured by TEM. XPS results showed an increase in carbon content on the solid after reduction, which was likely attributed to the formation of siderite (Figure S10 in Supporting Information S1). Siderite is also more susceptible to alteration or electron-beam dissolution, while magnetite remains structurally stable. Previous studies demonstrated that magnetite often serves as a transient Fe(III)-bearing intermediate and precursor for siderite formation (H. L. Dong et al., 2000; Fredrickson et al., 1998). The coexistence of nanoscale magnetite, siderite and possibly other poorly crystalline Fe(II)-bearing phases thus reflects a dynamic balance between Fe(II) generation, mineral transformation, and As retention. The persistence of aqueous Fe(II)-DFOB complexes likely delayed mineral maturation, sustaining fine-grained, amorphous Fe(II) phases with high As affinity. Adsorption of DFOB on goethite may have further modified Fe(II) gradients and interfacial electron transfer, shaping the sequence of mineral transformation. The resulting assemblage of nanomagnetite, siderite, and amorphous Fe(II) nanoparticles provided multiple sorption and coprecipitation sites for As, effectively counterbalancing DFOB-enhanced Fe(III) dissolution.

No change in As speciation was observed in either the As(V)-Gt or As(III)-Gt systems following microbial reduction, as indicated by XPS As3d spectra (Figure S11 in Supporting Information S1), indicating that *Shewanella oneidensis* MR-1 neither reduced As(V) nor oxidized As(III) under the experimental conditions (Jiang et al., 2009, 2013). Accordingly, As mobilization was controlled by desorption and redistribution associated with Fe(III) dissolution and secondary mineral formation, rather than direct microbial As redox transformation. HAADF-STEM-EDS mapping revealed close spatial overlap between As, Fe, and O (Figure S12, S13 in Supporting Information S1), confirming that As was associated with Fe-bearing phases rather than discrete precipitates. Facet-specific dissolution and localized Fe(II) nucleation created highly reactive surfaces that favored As retention. At circumneutral pH, DFOB-promoted dissolution can release As from reactive As-bearing goethite

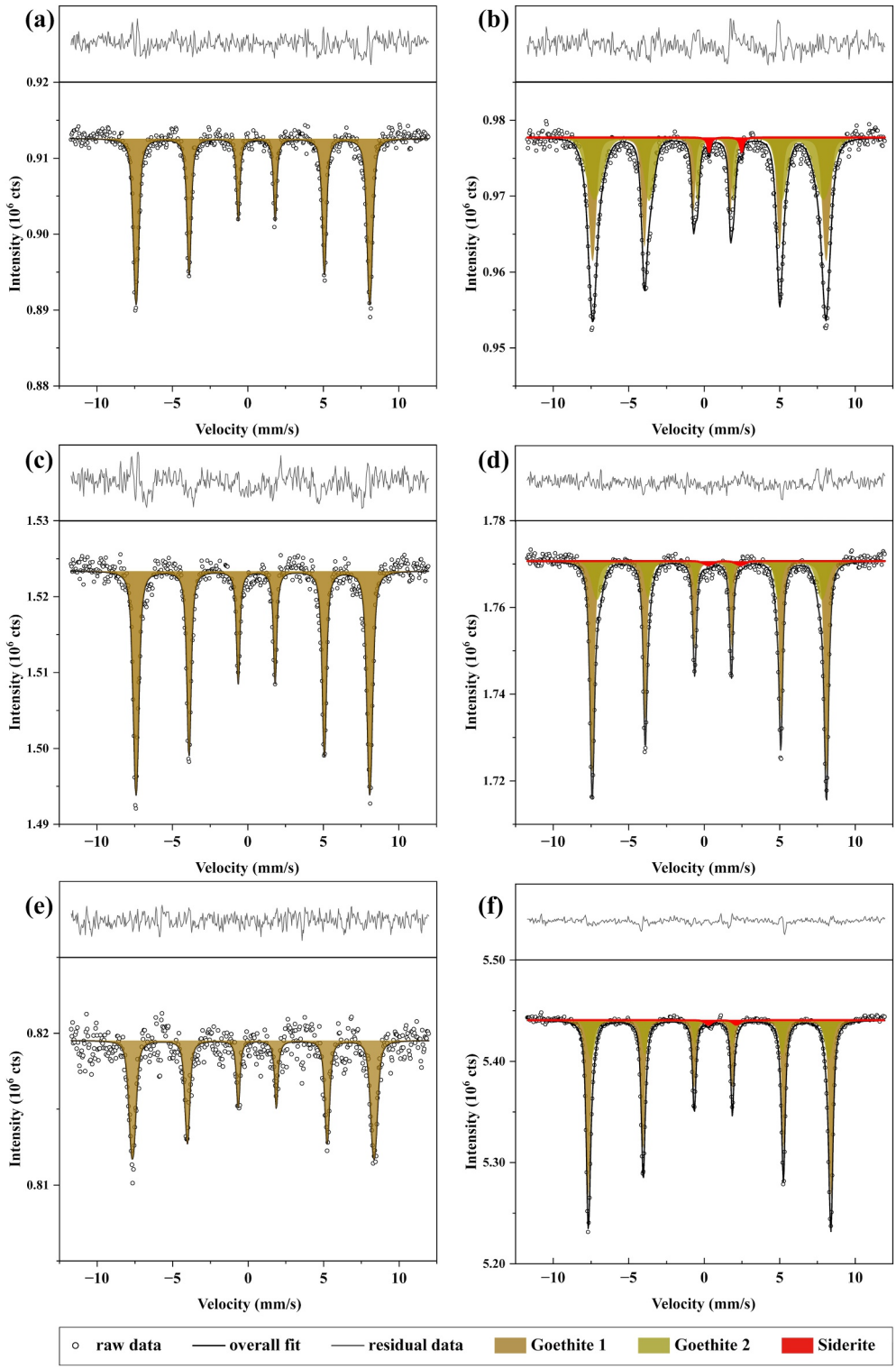

Figure 5. Mössbauer spectra of solid residues after microbial reduction, including residual plots and fitted spectra. Residuals, calculated as data minus fit, are shown in the upper panels, and the corresponding raw spectra with fitted components are shown in the lower panels. Spectra are shown for (a) Gt-MR-1, (b) Gt-MR-1-DFOB, (c) As(V)-Gt-MR-1, (d) As(V)-Gt-MR-1-DFOB at 140 K and (e) As(III)-Gt-MR-1 and (f) As(III)-Gt-MR-1-DFOB at 77 K. Fitted hyperfine parameters and relative areas of each site are provided in Table S4 in Supporting Information S1.

surfaces, while accumulated Fe(II) may interact with residual goethite surfaces and alter As partitioning. Therefore, retained As is more likely associated with a broader Fe-rich solid pool, including Fe(II)-modified residual goethite, associated Fe-rich surfaces, and newly formed Fe(II)-bearing secondary phases. At the end of microbial reduction, the difference between predicted and observed As concentrations indicated that approximately 40.7 μM As(V) was retained in the solid phase (Section 3.2). Comparison of this retained As with the formed solid-phase Fe(II) pool, estimated as the difference between total Fe(II) and dissolved Fe(II), yielded an As/Fe ratio of 0.07. This ratio was consistent with values reported for As incorporated into biogenic magnetite and siderite (C. H. Liu et al., 2015; X. Liu et al., 2015), validating that these nano particles possess sufficient sorptive capacity to account for the missing As and explaining the observed decoupling between Fe(III) reduction and As release in the MR-1-DFOB series.

In conclusion, these findings reveal the coupled mineralogical and geochemical processes governing Fe-As interactions during microbial Fe(III) reduction in the presence of DFOB. The siderophore DFOB enhanced microbial Fe(III) reduction by increasing Fe(III) bioavailability and facilitating electron transfer. Although DFOB also stimulated As release, the MR-1-DFOB treatments exhibited substantially greater Fe(III) reduction without a proportional increase in As mobilization compared to MR-1-only treatments. This decoupling indicates that secondary mineral formation, particularly nanoscale magnetite and minor siderite, played a critical role in limiting As release by providing additional solid-phase sinks. These findings provide mechanistic insight into As mobility in reducing aquifers, where DOM transformation, microbial Fe(III) reduction, Fe mineral transformation, and As enrichment often occur concurrently (Glodowska et al., 2020; Mladenov et al., 2015). The effect of individual siderophores may be attenuated because their concentrations in groundwater are typically low (Kim et al., 2009; Tomczyk-Żak et al., 2013). However, DOM contains diverse organic ligands, including humic substances, low-molecular-weight organic acids, and functional groups with strong Fe-binding or redox-active properties. These compounds may influence Fe(III) mineral dissolution, Fe(II) complexation, microbial Fe reduction, and secondary mineral formation. Moreover, sediments from many high-As aquifers contain multiple Fe(III) (oxyhydr) oxides, such as ferrihydrite, goethite, and hematite (Guo, Liu, et al., 2013; Li et al., 2023). These minerals may transform through different pathways and generate a range of secondary phases, including magnetite, siderite, vivianite, green rust, and Fe sulfides (Y. R. Dong et al., 2020; Han et al., 2018). These secondary minerals may either sequester As through adsorption or structural incorporation or release As when mineral transformation is incomplete or sorption sites are limited. Therefore, although our model system does not directly reproduce the full complexity of natural aquifers, it highlights a key mechanism by which Fe-binding organic ligands may enhance Fe cycling without necessarily causing proportional As mobilization.

4. Conclusions

This study demonstrates that strong Fe-complexing organic ligands can decouple microbial Fe(III) reduction from arsenic mobilization during the bioreductive dissolution of As-bearing goethite. The hydroxamate siderophore desferrioxamine B (DFOB) substantially enhanced both the rate and extent of Fe(III) reduction by *Shewanella oneidensis* MR-1 through ligand-promoted Fe(III) complexation and improved microbe-mineral electron transfer. Arsenic release was closely linked to the amount of reacted Fe, confirming Fe-As redox cycling during microbial reduction. However, despite strongly stimulating Fe(III) reduction, DFOB did not increase As mobilization relative to MR-1-only series. This behavior was attributed to the DFOB-induced redistribution of biogenic Fe(II) into secondary Fe-rich phases, such as locally observed nano-magnetite, minor siderite, and possibly poorly crystalline Fe(II)-bearing phases, which may have contributed to As retention via adsorption and coprecipitation. These findings highlight a previously underappreciated role of Fe-binding organic ligands in promoting the formation of As-sequestering mineral phases, thereby limiting As mobility under reducing conditions. The results provide new insight into the complex role of DOM in regulating Fe-As interactions and improve our understanding of As behavior in redox-active groundwater systems.

Conflict of Interest

The authors declare no conflicts of interest relevant to this study.

Availability Statement

Experimental data sets of microbial Fe(III) reduction by *Shewanella oneidensis* MR-1 with and without DFOB related to this study are available at the Mendeley open repository (Li & Xiu, 2026).

Acknowledgments
The work is financially supported by the National Natural Science Foundation of China (W2511041, 42130509, and 42202293), National Key Research and Development Program of China (Grant 2021YFA0715902), 111 projects (B20010), the Fundamental Research Funds for the Central Universities (590223006). W.X. gratefully acknowledges support from the Alexander von Humboldt Foundation through a Humboldt Research Fellowship for experienced researchers.

References

Aftabtalab, A., Rinklebe, J., Shaheen, S. M., Niazi, N. K., Moreno-Jiménez, E., Schaller, J., & Knorr, K. H. (2022). Review on the interactions of arsenic, iron (oxy)(hydr)oxides, and dissolved organic matter in soils, sediments, and groundwater in a ternary system. *Chemosphere*, *286*, 131790. https://doi.org/10.1016/j.chemosphere.2021.131790

Amonette, J. E., & Templeton, J. C. (1998). Improvements to the quantitative assay of nonrefractory minerals for Fe(II) and total Fe using 1,10-phenanthroline. *Clays and Clay Minerals*, *46*(1), 51–62. https://doi.org/10.1346/CCMN.1998.0460106

Amstaetter, K., Borch, T., & Kappler, A. (2012). Influence of humic acid imposed changes of ferrihydrite aggregation on microbial Fe(III) reduction. *Geochimica et Cosmochimica Acta*, *85*, 326–341. https://doi.org/10.1016/j.gca.2012.02.003

Amstaetter, K., Borch, T., Larese-Casanova, P., & Kappler, A. (2010). Redox transformation of arsenic by Fe(II)-Activated goethite (α-FeOOH). *Environmental Science & Technology*, *44*(1), 102–108. https://doi.org/10.1021/es901274s

Barrón, V., & Torrent, J. (1996). Surface hydroxyl configuration of various crystal faces of hematite and goethite. *Journal of Colloid and Interface Science*, *177*(2), 407–410. https://doi.org/10.1006/jcis.1996.0051

Bellotti, D., & Remelli, M. (2021). Deferoxamine B: A natural, excellent and versatile metal chelator. *Molecules*, *26*(11), 3255. https://doi.org/10.3390/molecules26113255

Biswakarma, J., Kang, K., Borowski, S. C., Schenkeveld, W. D. C., Kraemer, S. M., Hering, J. G., & Hug, S. J. (2019). Fe(II)-Catalyzed ligand-controlled dissolution of iron(hydr)oxides. *Environmental Science & Technology*, *53*(1), 88–97. https://doi.org/10.1021/acs.est.8b03910

Biswakarma, J., Kang, K., Schenkeveld, W. D. C., Kraemer, S. M., Hering, J. G., & Hug, S. J. (2020). Linking isotope exchange with Fe(II)-Catalyzed dissolution of iron(hydr)oxides in the presence of the bacterial siderophore Desferrioxamine-B. *Environmental Science & Technology*, *54*(2), 768–777. https://doi.org/10.1021/acs.est.9b04235

Biswakarma, J., Kang, K., Schenkeveld, W. D. C., Kraemer, S. M., Hering, J. G., & Hug, S. J. (2021). Catalytic effects of photogenerated Fe(II) on the ligand-controlled dissolution of Iron(hydr)oxides by EDTA and DFOB. *Chemosphere*, *263*, 128188. https://doi.org/10.1016/j.chemosphere.2020.128188

Boiteau, R. M., Mende, D. R., Hawco, N. J., McIlvin, M. R., Fitzsimmons, J. N., Saito, M. A., et al. (2016). Siderophore-based microbial adaptations to iron scarcity across the eastern Pacific Ocean. *Proceedings of the National Academy of Sciences*, *113*(50), 14237–14242. https://doi.org/10.1073/pnas.1608594113

Boukhalfa, H., & Crumbliss, A. L. (2002). Chemical aspects of siderophore mediated iron transport. *Biometals*, *15*(4), 325–339. https://doi.org/10.1023/A:1020218608266

Cai, X. L., ThomasArrigo, L. K., Fang, X., Bouchet, S., Cui, Y. S., & Kretzschmar, R. (2021). Impact of organic matter on microbially-mediated reduction and mobilization of arsenic and iron in arsenic(V)-bearing ferrihydrite. *Environmental Science & Technology*, *55*(2), 1319–1328. https://doi.org/10.1021/acs.est.0c05329

Carrasco, N., Kretzschmar, R., Pesch, M. L., & Kraemer, S. M. (2007). Low concentrations of surfactants enhance siderophore-promoted dissolution of goethite. *Environmental Science & Technology*, *41*(10), 3633–3638. https://doi.org/10.1021/es062897r

Cheah, S. F., Kraemer, S. M., Cervini-Silva, J., & Sposito, G. (2003). Steady-state dissolution kinetics of goethite in the presence of desferrioxamine B and oxalate ligands: Implications for the microbial acquisition of iron. *Chemical Geology*, *198*(1–2), 63–75. https://doi.org/10.1016/S0009-2541(02)00421-7

Ding, L. J., Li, X. M., Wang, Y. F., Luo, C. Y., Wang, X. D., Duan, G. L., & Zhu, Y. G. (2022). Influences of arsenate and/or phosphate adsorption to ferrihydrite on iron-reducing and arsenic-reducing microbial communities in paddy soil revealed by rRNA-13C-acetate probing. *Soil Biology and Biochemistry*, *169*, 108679. https://doi.org/10.1016/j.soilbio.2022.108679

Ding, Y. F., Sheng, A. X., Li, X., Liu, Y. Y., Yan, M. Q., Takahashi, Y., & Liu, J. (2024). Triplet-excited riboflavin promotes labile Fe(III) accumulation and changes mineralization pathways in Fe(II)-Catalyzed ferrihydrite transformation. *Environmental Science & Technology*, *58*(50), 22148–22158. https://doi.org/10.1021/acs.est.4c08589

Dixit, S., & Hering, J. G. (2003). Comparison of Arsenic(V) and Arsenic(III) sorption onto iron oxide minerals: Implications for arsenic mobility. *Environmental Science & Technology*, *37*(18), 4182–4189. https://doi.org/10.1021/es030309t

Dong, H. L., Fredrickson, J. K., Kennedy, D. W., Zachara, J. M., Kukkadapu, R. K., & Onstott, T. C. (2000). Mineral transformations associated with the microbial reduction of magnetite. *Chemical Geology*, *169*(3–4), 299–318. https://doi.org/10.1016/S0009-2541(00)00210-2

Dong, H. L., Zeng, Q., Sheng, Y. Z., Chen, C. M., Yu, G. H., & Kappler, A. (2023). Coupled iron cycling and organic matter transformation across redox interfaces. *Nature Reviews Earth & Environment*, *4*(9), 659–673. https://doi.org/10.1038/s43017-023-00470-5

Dong, Y. R., Sanford, R. A., Boyanov, M. I., Flynn, T. M., O'Loughlin, E. J., Kemner, K. M., et al. (2020). Controls on iron reduction and biomineralization over broad environmental conditions as suggested by the firmicutes *Orenia metallireducens* strain Z6. *Environmental Science & Technology*, *54*(16), 10128–10140. https://doi.org/10.1021/acs.est.0c03853

Feng, X. J., Li, Y., Jin, J. Y., Qiao, W., Gao, Z. P., & Guo, H. M. (2025). Electrochemistry and molecular compositions reflect electron shuttling of dissolved organic matter in high arsenic groundwater. *Environmental Science & Technology*, *59*(17), 8591–8601. https://doi.org/10.1021/acs.est.4c13575

Fredrickson, J. K., Zachara, J. M., Kennedy, D. W., Dong, H., Onstott, T. C., Hinman, N. W., & Li, S. (1998). Biogenic iron mineralization accompanying the dissimilatory reduction of hydrous ferric oxide by a groundwater bacterium. *Geochimica et Cosmochimica Acta*, *62*(19–20), 3239–3257. https://doi.org/10.1016/S0016-7037(98)00243-9

Fritzsche, A., Bosch, J., Sander, M., Schröder, C., Byrne, J. M., Ritschel, T., et al. (2021). Organic matter from redoximorphic soils accelerates and sustains microbial Fe(III) reduction. *Environmental Science & Technology*, *55*(15), 10821–10831. https://doi.org/10.1021/acs.est.1c01183

Gimenez, J., Martinez, M., Depablo, J., Rovira, M., & Duro, L. (2007). Arsenic sorption onto natural hematite, magnetite, and goethite. *Journal of Hazardous Materials*, *141*(3), 575–580. https://doi.org/10.1016/j.jhazmat.2006.07.020

Glodowska, M., Stopelli, E., Schneider, M., Lightfoot, A., Rathi, B., Straub, D., et al. (2020). Role of in situ natural organic matter in mobilizing as during microbial reduction of Fe^{III}-Mineral-Bearing aquifer sediments from hanoi (Vietnam). *Environmental Science & Technology*, *54*(7), 4149–4159. https://doi.org/10.1021/acs.est.9b07183

Guo, H. M., Li, Y., Zhao, K., Ren, Y., & Wei, C. (2011). Removal of arsenite from water by synthetic siderite: Behaviors and mechanisms. *Journal of Hazardous Materials*, *186*(2–3), 1847–1854. https://doi.org/10.1016/j.jhazmat.2010.12.078

Guo, H. M., Liu, C., Lu, H., Wanty, R. B., Wang, J., & Zhou, Y. Z. (2013). Pathways of coupled arsenic and iron cycling in high arsenic groundwater of the hetao basin, Inner Mongolia, China: An iron isotope approach. *Geochimica et Cosmochimica Acta*, *112*, 130–145. https://doi.org/10.1016/j.gca.2013.02.031

Guo, H. M., Liu, Z. Y., Ding, S. S., Hao, C. B., Xiu, W., & Hou, W. G. (2015). Arsenate reduction and mobilization in the presence of Indigenous aerobic bacteria obtained from high arsenic aquifers of the Hetao basin, Inner Mongolia. *Environmental Pollution*, *203*, 50–59. https://doi.org/10.1016/j.envpol.2015.03.034

Guo, H. M., Ren, Y., Liu, Q., Zhao, K., & Li, Y. (2013). Enhancement of arsenic adsorption during mineral transformation from siderite to goethite: Mechanism and application. *Environmental Science & Technology*, *47*(2), 1009–1016. https://doi.org/10.1021/es303503m

Han, R., Liu, T. X., Li, F. B., Li, X. M., Chen, D. D., & Wu, Y. D. (2018). Dependence of secondary mineral formation on Fe(II) production from ferrihydrite reduction by Shewanella oneidensis MR-1. *ACS Earth and Space Chemistry*, *2*(4), 399–409. https://doi.org/10.1021/acsearthspacechem.7b00132

Han, X. H., Wang, F. X., Zheng, S. L., Qiu, H., Liu, Y., Wang, J., et al. (2024). Morphological, microstructural, and in situ chemical characteristics of siderite produced by iron-reducing bacteria. *Environmental Science & Technology*, *58*(25), 11016–11026. https://doi.org/10.1021/acs.est.3c10988

Hua, J., Feng, C. H., Sun, J., Wu, F., Wu, F., & Liu, C. S. (2022). Facet-preferential reduction of hematite nanocrystals by *Shewanella oneidensis* MR-1: An iron isotope tracer study. *Chemical Geology*, *614*, 121166. https://doi.org/10.1016/j.chemgeo.2022.121166

Huang, Y. H., Zhao, X. P., Wang, X. H., Gao, B., Oyama, K., Tokoro, C., et al. (2024). Insights on the contradiction between the affinity and capacity of ferrihydrite toward As(III) and As(V): Surface reaction revisited. *Environmental Science & Technology*, *58*, 15257–15267. https://doi.org/10.1021/acs.est.4c05795

Jaisi, D. P., Dong, H. L., & Liu, C. X. (2007). Influence of biogenic Fe(II) on the extent of microbial reduction of Fe(III) in clay minerals nontronite, illite, and chlorite. *Geochimica et Cosmochimica Acta*, *71*(5), 1145–1158. https://doi.org/10.1016/j.gca.2006.11.027

Jiang, S. H., Lee, J. H., Kim, M. G., Myung, N. V., Fredrickson, J. K., Sadowsky, M. J., & Hur, H. G. (2009). Biogenic formation of As-S nanotubes by diverse shewanella strains. *Applied and Environmental Microbiology*, *75*(21), 6896–6899. https://doi.org/10.1128/AEM.00450-09

Jiang, S. H., Lee, J. H., Kim, D., Kanaly, R. A., Kim, M. G., & Hur, H. G. (2013). Differential arsenic mobilization from As-Bearing ferrihydrite by iron-respiring *Shewanella* strains with different arsenic-reducing activities. *Environmental science & technology*, 130710112631007. https://doi.org/10.1021/es400534z

Kanematsu, M., Young, T. M., Fukushi, K., Green, P. G., & Darby, J. L. (2013). Arsenic(III, V) adsorption on a goethite-based adsorbent in the presence of major co-existing ions: Modeling competitive adsorption consistent with spectroscopic and molecular evidence. *Geochimica et Cosmochimica Acta*, *106*, 404–428. https://doi.org/10.1016/j.gca.2012.09.055

Kim, D., Duckworth, O. W., & Strathmann, T. J. (2009). Hydroxamate siderophore-promoted reactions between iron(II) and nitroaromatic groundwater contaminants. *Geochimica et Cosmochimica Acta*, *73*(5), 1297–1311. https://doi.org/10.1016/j.gca.2008.11.039

Kim, D., Duckworth, O. W., & Strathmann, T. J. (2010). Reactions of aqueous iron–DFOB (desferrioxamine B) complexes with flavin mononucleotide in the absence of strong iron(II) chelators. *Geochimica et Cosmochimica Acta*, *74*(5), 1513–1529. https://doi.org/10.1016/j.gca.2009.12.020

Klyukin, K., Rosso, K. M., & Alexandrov, V. (2018). Iron dissolution from goethite (α-FeOOH) surfaces in water by ab initio enhanced free-energy simulations. *The Journal of Physical Chemistry C*, *122*(28), 16086–16091. https://doi.org/10.1021/acs.jpcc.8b03743

Kramer, J., Özkaya, Ö., & Kümmerli, R. (2020). Bacterial siderophores in community and host interactions. *Nature Reviews Microbiology*, *18*(3), 152–163. https://doi.org/10.1038/s41579-019-0284-4

Kuhn, K. M., Maurice, P. A., Neubauer, E., Hofmann, T., & Von der Kammer, F. (2014). Accessibility of humic-associated Fe to a microbial siderophore: Implications for bioavailability. *Environmental Science & Technology*, *48*(2), 1015–1022. https://doi.org/10.1021/es404186v

Kuzmann, E., Nagy, S., & Vértes, A. (2003). Critical review of analytical applications of mössbauer spectroscopy illustrated by mineralogical and geological examples (IUPAC technical report). *Pure and Applied Chemistry*, *75*(6), 801–858. https://doi.org/10.1351/pac200375060801

Latta, D. E., Bachman, J. E., & Scherer, M. M. (2012). Fe electron transfer and atom exchange in goethite: Influence of Al-Substitution and anion sorption. *Environmental Science & Technology*, *46*(19), 10614–10623. https://doi.org/10.1021/es302094a

Li, S. M., & Xiu, W. (2026). Siderophores reshape microbial Fe(III) reduction and arsenic release from iron (oxyhydr)oxides (version 1) [Dataset]. *Mendeley Data*. https://doi.org/10.17632/XXBJK8VBJN.1

Li, S. M., Xiu, W., Liu, X., Fang, Z. X., Lloyd, J. R., & Guo, H. M. (2025). Ligand exchange by As(V) enhanced desferrioxamine B-induced goethite dissolution: Insights into as mobilization in groundwater systems. *Applied Geochemistry*, *187*, 106412. https://doi.org/10.1016/j.apgeochem.2025.106412

Li, Y., Guo, H. M., Gao, Z. P., Ke, T. T., Zhu, Z. J., Cao, Y. Y., et al. (2023). Phosphorus in shallow and deep groundwater: Importance of P/Fe ratio in Fe(III) oxides in aquifer sediments. *Journal of Hydrology*, *623*, 129860. https://doi.org/10.1016/j.jhydrol.2023.129860

Liu, C. H., Chuang, Y. H., Chen, T. Y., Tian, Y., Li, H., Wang, M. K., & Zhang, W. (2015). Mechanism of arsenic adsorption on magnetite nanoparticles from water: Thermodynamic and spectroscopic studies. *Environmental Science & Technology*, *49*(13), 7726–7734. https://doi.org/10.1021/acs.est.5b00381

Liu, J., Sheng, A. X., Li, X. X., Arai, Y., Ding, Y. F., Nie, M. J., et al. (2022). Understanding the importance of labile Fe(III) during Fe(II)-Catalyzed transformation of metastable iron oxyhydroxides. *Environmental Science & Technology*, *56*(6), 3801–3811. https://doi.org/10.1021/acs.est.1c08044

Liu, X., Fu, J. W., Da Silva, E., Shi, X. X., Cao, Y., Rathinasabapathi, B., et al. (2017). Microbial siderophores and root exudates enhanced goethite dissolution and Fe/As uptake by As-hyperaccumulator *Pteris vittata*. *Environmental Pollution*, *223*, 230–237. https://doi.org/10.1016/j.envpol.2017.01.016

Liu, X., Yang, G. M., Guan, D. X., Ghosh, P., & Ma, L. Q. (2015). Catecholate-siderophore produced by As-resistant bacterium effectively dissolved $FeAsO_4$ and promoted *Pteris vittata* growth. *Environmental Pollution*, *206*, 376–381. https://doi.org/10.1016/j.envpol.2015.07.034

Livi, K. J. T., Villalobos, M., Leary, R., Varela, M., Barnard, J., Villacís-García, M., et al. (2017). Crystal face distributions and surface site densities of two synthetic goethites: Implications for adsorption capacities as a function of particle size. *Langmuir*, *33*(36), 8924–8932. https://doi.org/10.1021/acs.langmuir.7b01814

Livi, K. J. T., Villalobos, M., Ramasse, Q., Brydson, R., & Salazar-Rivera, H. S. (2023). Surface site density of synthetic goethites and its relationship to atomic surface roughness and crystal size. *Langmuir*, *39*(1), 556–562. https://doi.org/10.1021/acs.langmuir.2c02818

Lopez-Adams, R., Newsome, L., Moore, K. L., Lyon, I. C., & Lloyd, J. R. (2021). Dissimilatory Fe(III) reduction controls on arsenic mobilization: A combined biogeochemical and NanoSIMS imaging approach. *Frontiers in Microbiology*, *12*, 640734. https://doi.org/10.3389/fmicb.2021.640734

Lovley, D. R. (1991). Magnetite formation during microbial dissimilatory iron reduction. In R. B. Frankel & R. P. Blakemore (Eds.), *Iron biominerals* (pp. 151–166). Springer. https://doi.org/10.1007/978-1-4615-3810-3_11

Majzlan, J. (2011). Thermodynamic stabilization of hydrous ferric oxide by adsorption of phosphate and arsenate. *Environmental Science & Technology*, *45*(11), 4726–4732. https://doi.org/10.1021/es1040249

Melton, E. D., Swanner, E. D., Behrens, S., Schmidt, C., & Kappler, A. (2014). The interplay of microbially mediated and abiotic reactions in the biogeochemical Fe cycle. *Nature Reviews Microbiology*, *12*, 797–808. https://doi.org/10.1038/nrmicro3347

Mladenov, N., Zheng, Y., Simone, B., Bilinski, T. M., McKnight, D. M., Nemergut, D., et al. (2015). Dissolved organic matter quality in a shallow aquifer of Bangladesh: Implications for arsenic mobility. *Environmental Science & Technology*, *49*(18), 10815–10824. https://doi.org/10.1021/acs.est.5b01962

Muehe, E. M., Scheer, L., Daus, B., & Kappler, A. (2013). Fate of arsenic during microbial reduction of biogenic versus abiogenic As–Fe(III)–Mineral coprecipitates. *Environmental Science & Technology*, *47*, 8297–8307. https://doi.org/10.1021/es400801z

Mukherjee, A., Coomar, P., Sarkar, S., Johannesson, K. H., Fryar, A. E., Schreiber, M. E., et al. (2024). Arsenic and other geogenic contaminants in global groundwater. *Nature Reviews Earth & Environment*, *5*(4), 312–328. https://doi.org/10.1038/s43017-024-00519-z

Murad, E., & Cashion, J. (2004). *Mössbauer spectroscopy of environmental materials and their industrial utilization*. Springer. https://doi.org/10.1007/978-1-4419-9040-2

O'Loughlin, E. J., Boyanov, M. I., Flynn, T. M., Gorski, C. A., Hofmann, S. M., McCormick, M. L., et al. (2013). Effects of bound phosphate on the bioreduction of lepidocrocite (γ-FeOOH) and maghemite (γ-Fe_2O_3) and formation of secondary minerals. *Environmental Science & Technology*, *47*(16), 9157–9166. https://doi.org/10.1021/es400627j

O'Reilly, S. E., Strawn, D. G., & Sparks, D. L. (2001). Residence time effects on arsenate adsorption/desorption mechanisms on goethite. *Soil Science Society of America Journal*, *65*(1), 67–77. https://doi.org/10.2136/sssaj2001.65167x

Perez-Gonzalez, T., Jimenez-Lopez, C., Neal, A. L., Rull-Perez, F., Rodriguez-Navarro, A., Fernandez-Vivas, A., & Iañez-Pareja, E. (2010). Magnetite biomineralization induced by *Shewanella oneidensis*. *Geochimica et Cosmochimica Acta*, *74*(3), 967–979. https://doi.org/10.1016/j.gca.2009.10.035

Piepenbrock, A., Dippon, U., Porsch, K., Appel, E., & Kappler, A. (2011). Dependence of microbial magnetite formation on humic substance and ferrihydrite concentrations. *Geochimica et Cosmochimica Acta*, *75*(22), 6844–6858. https://doi.org/10.1016/j.gca.2011.09.007

Pinchuk, G. E., Geydebrekht, O. V., Hill, E. A., Reed, J. L., Konopka, A. E., Beliaev, A. S., & Fredrickson, J. K. (2011). Pyruvate and lactate metabolism by *Shewanella oneidensis* MR-1 under fermentation, oxygen limitation, and fumarate respiration conditions. *Applied and Environmental Microbiology*, *77*(23), 8234–8240. https://doi.org/10.1128/AEM.05382-11

Podgorski, J., & Berg, M. (2020). Global threat of arsenic in groundwater. *Science*, *368*(6493), 845–850. https://doi.org/10.1126/science.aba1510

Qiao, W., Guo, H. M., He, C., Shi, Q., Xing, S. P., & Gao, Z. P. (2021). Identification of processes mobilizing organic molecules and arsenic in geothermal confined groundwater from Pliocene aquifers. *Water Research*, *198*, 117140. https://doi.org/10.1016/j.watres.2021.117140

Reichard, P. U., Kretzschmar, R., & Kraemer, S. M. (2007). Dissolution mechanisms of goethite in the presence of siderophores and organic acids. *Geochimica et Cosmochimica Acta*, *71*(23), 5635–5650. https://doi.org/10.1016/j.gca.2006.12.022

Roden, E. E., & Urrutia, M. M. (2002). Influence of biogenic Fe(II) on bacterial crystalline Fe(III) oxide reduction. *Geomicrobiology Journal*, *19*(2), 209–251. https://doi.org/10.1080/01490450252864280

Rubasinghege, G., Lentz, R. W., Scherer, M. M., & Grassian, V. H. (2010). Simulated atmospheric processing of iron oxyhydroxide minerals at low pH: Roles of particle size and acid anion in iron dissolution. *Proceedings of the National Academy of Sciences*, *107*(15), 6628–6633. https://doi.org/10.1073/pnas.0910809107

Schwertmann, U., & Cornell, R. M. (2000). Iron oxides in the laboratory: Preparation and characterization. In *2nd completely rev. And extended ed*. Wiley VCH.

Shen, S. W., Li, X. F., Cullen, W. R., Weinfeld, M., & Le, X. C. (2013). Arsenic binding to proteins. *Chemistry Review*, *113*(10), 7769–7792. https://doi.org/10.1021/cr300015c

Sheng, A. X., Deng, Y. R., Ding, Y. F., Cheng, L. X., Liu, Y. Y., Li, X. X., et al. (2024). Regulation of ferrihydrite biotransformation by Fe(II) supply rates and extracellular polymeric substances. *Geochimica et Cosmochimica Acta*, *385*, 87–99. https://doi.org/10.1016/j.gca.2024.08.029

Sheng, A. X., Li, X. X., Arai, Y., Ding, Y. F., Rosso, K. M., & Liu, J. (2020). Citrate controls Fe(II)-catalyzed transformation of ferrihydrite by complexation of the labile Fe(III) intermediate. *Environmental Science & Technology*, *54*(12), 7309–7319. https://doi.org/10.1021/acs.est.0c00996

Simanova, A. A., Persson, P., & Loring, J. S. (2010). Evidence for ligand hydrolysis and Fe(III) reduction in the dissolution of goethite by Desferrioxamine-B. *Geochimica et Cosmochimica Acta*, *74*(23), 6706–6720. https://doi.org/10.1016/j.gca.2010.08.037

Spasojević, I., Armstrong, S. K., Brickman, T. J., & Crumbliss, A. L. (1999). Electrochemical behavior of the Fe(III) complexes of the cyclic hydroxamate siderophores alcaligin and desferrioxamine E. *Inorganic Chemistry*, *38*(3), 449–454. https://doi.org/10.1021/ic980635n

Stookey, L. L. (1970). Ferrozine-a new spectrophotometric reagent for iron. *Analytical Chemistry*, *42*(7), 779–781. https://doi.org/10.1021/ac60289a016

ThomasArrigo, L. K., Byrne, J. M., Kappler, A., & Kretzschmar, R. (2018). Impact of organic matter on iron(II)-catalyzed mineral transformations in ferrihydrite–organic matter coprecipitates. *Environmental Science & Technology*, *52*(21), 12316–12326. https://doi.org/10.1021/acs.est.8b03206

Tomczyk-Żak, K., Kaczanowski, S., Drewniak, Ł., Dmoch, Ł., Sklodowska, A., & Zielenkiewicz, U. (2013). Bacteria diversity and arsenic mobilization in rock biofilm from an ancient gold and arsenic mine. *Science of the Total Environment*, *461–462*, 330–340. https://doi.org/10.1016/j.scitotenv.2013.04.087

Tufano, K. J., & Fendorf, S. (2008). Confounding impacts of iron reduction on arsenic retention. *Environmental Science & Technology*, *42*(13), 4777–4783. https://doi.org/10.1021/es702625e

Urrutia, M. M., Roden, E. E., & Zachara, J. M. (1999). Influence of aqueous and solid-phase Fe(II) complexants on microbial reduction of crystalline Iron(III) oxides. *Environmental Science & Technology*, *33*(22), 4022–4028. https://doi.org/10.1021/es990447b

Usman, M., Abdelmoula, M., Faure, P., Ruby, C., & Hanna, K. (2013). Transformation of various kinds of goethite into magnetite: Effect of chemical and surface properties. *Geoderma*, *197–198*, 9–16. https://doi.org/10.1016/j.geoderma.2012.12.015

Usman, M., Byrne, J. M., Chaudhary, A., Orsetti, S., Hanna, K., Ruby, C., et al. (2018). Magnetite and green rust: Synthesis, properties, and environmental applications of mixed-valent iron minerals. *Chemistry Review*, *118*(7), 3251–3304. https://doi.org/10.1021/acs.chemrev.7b00224

Wang, J., Wu, M. Y., Lu, G., & Si, Y. B. (2016). Biotransformation and biomethylation of arsenic by *Shewanella oneidensis* MR-1. *Chemosphere*, *145*, 329–335. https://doi.org/10.1016/j.chemosphere.2015.11.107

Wang, Y. X., Li, J. X., Ma, T., Xie, X. J., Deng, Y. M., & Gan, Y. Q. (2021). Genesis of geogenic contaminated groundwater: As, F and I. *Critical Reviews in Environmental Science and Technology*, *51*(24), 2895–2933. https://doi.org/10.1080/10643389.2020.1807452

Wang, Z. M., Scnkeveld, W. D. C., Kraemer, S. M., & Giammar, D. E. (2015). Synergistic effect of reductive and ligand-promoted dissolution of goethite. *Environmental Science & Technology*, *49*, 7236–7244. https://doi.org/10.1021/acs.est.5b01191

Wu, S., Fang, G. D., Wang, D. J., Jaisi, D. P., Cui, P. X., Wang, R., et al. (2018). Fate of As(III) and As(V) during microbial reduction of arsenic-bearing ferrihydrite facilitated by activated carbon. *ACS Earth and Space Chemistry*, *2*(9), 878–887. https://doi.org/10.1021/acsearthspacechem.8b00058

Xu, X. Y., Mansor, M., Li, G. X., Chiu, T. H., Haderlein, S. B., Kappler, A., & Joshi, P. (2025). Size-Dependent reduction kinetics of iron oxides in single and mixed mineral systems. *Environmental Science & Technology*, *59*(5), 2519–2530. https://doi.org/10.1021/acs.est.4c08032

Yean, S., Cong, L., Yavuz, C. T., Mayo, J. T., Yu, W. W., Kan, A. T., et al. (2005). Effect of magnetite particle size on adsorption and desorption of arsenite and arsenate. *Journal of Materials Research*, *20*(12), 3255–3264. https://doi.org/10.1557/jmr.2005.0403

Yu, W. T., Gao, Z. P., & Guo, H. M. (2024). Purification of As(III) through oxidation of siderite and As(III) by dissolved oxygen: Behavior and mechanism. *Environmental Science Nano*, *11*(5), 2145–2156. https://doi.org/10.1039/D3EN00974B

Yu, W. T., Cao, Y. Y., Yan, S., & Guo, H. M. (2023). New insights into arsenate removal during siderite oxidation by dissolved oxygen. *Science of the Total Environment*, *882*, 163556. https://doi.org/10.1016/j.scitotenv.2023.163556

Yu, W. T., Guo, H. M., & Hou, C. S. (2022). Removal of arsenate from aqueous solution by synthetic siderite-modified biochar: Characteristics and mechanisms. *Water, Air, & Soil Pollution*, *233*(7), 278. https://doi.org/10.1007/s11270-022-05750-2

Zachara, J. M., Fredrickson, J. K., Li, S.-M., Kennedy, D. W., Smith, S. C., & Gassman, P. L. (1998). Bacterial reduction of crystalline Fe (super 3+) oxides in single phase suspensions and subsurface materials. *American Mineralogist*, *83*(11–12 Part 2), 1426–1443. https://doi.org/10.2138/am-1998-11-1232

Zhang, L. M., Dong, H. L., Li, R. J., Liu, D., Bian, L., Chen, Y., et al. (2022). Effect of siderophore DFOB on U(VI) adsorption to clay mineral and its subsequent reduction by an iron-reducing bacterium. *Environmental Science & Technology*, *56*(17), 12702–12712. https://doi.org/10.1021/acs.est.2c02047

Zhang, Y. C., Liu, X. D., Cheng, J., & Lu, X. C. (2021). Interfacial structures and acidity constants of goethite from first-principles molecular dynamics simulations. *American Mineralogist*, *106*(11), 1736–1743. https://doi.org/10.2138/am-2021-7835